# A Signal Detection Strategy for the SETI All Sky Survey

J. Solomon and W. Lawton
Image Processing Applications and Development Section

M. P. Quirk
Communications Systems Research Section

E. T. Olsen
Space Physics and Astrophysics Section

*This article describes a source detection strategy for the SETI All Sky Survey. The method is designed to detect continuous wave (or very narrowband) sources transiting an antenna beam. The short-time spectra of the received signal are accumulated, and candidate extraterrestrial sources are recognized by the presence of narrowband power exceeding a threshold function. The threshold function is derived using a Neyman-Pearson hypothesis test.*

## I. Introduction

The NASA program for the Search for Extraterrestrial Intelligence (SETI) is currently developing prototype signal processing hardware and software, search strategies, and observing procedures for an ambitious search to be conducted in the early 1990's. The long range NASA SETI plan calls for an All Sky Survey covering the 1–10 GHz frequency range and a Targeted Search covering the 1–3 GHz frequency range. In the All Sky Survey, all $4\pi$ steradians of the celestial sphere will be surveyed with approximately uniform sensitivity for the presence of narrowband signals of extraterrestrial origin. In the Targeted Search, a thousand candidate sources will be observed, including nearby solar-type stars and interesting sources identified by the All Sky Survey.

The JPL SETI team has the responsibility for designing, developing, and implementing the All Sky Survey. To detect ETI signals, which are assumed to be narrowband, we divide the input bandwidth into narrowband channels using a Fast Fourier Transform (FFT). The FFT output power in each channel is accumulated and convolved with a filter matched to the antenna beam shape. A thresholding operation is performed on the matched-filter output to locate channels with excess power. These events are stored for a confirmation test on the return scan. The processing up to and including the matched filter is performed in a high-speed digital spectrum analyzer such as that described in Ref. 1. A digital computer system will detect ETI signals from the spectrum analyzer output.

This report presents the current design for the signal detection strategy. In the next section we describe the All Sky Survey. Section III describes the signal characteristics, and in Section IV we derive the performance characteristics for a Neyman-Pearson detection system applied to these signals.

## II. The SETI All Sky Survey

The characteristics of the All Sky Survey are shown in Table 1. The basic premise of the Sky Survey is that we do not know where to look. There are over a million solar-type stars within a thousand light years of the earth, and their density per unit steradian is approximately uniform. Since we also do not know how strong a signal might be, there is no preferred direction within this volume of stars.

To satisfy the first three characteristics, the antenna beam must be swept across the sky at 20 to 50 times the sidereal rate. The sensitivity of the survey is thereby established (within an order of magnitude), and the class of signal types is restricted to Continuous Wave (CW) and narrowband signals with bandwidths from 10 to 30 Hz.

The requirement of uniform sensitivity affects the signal detection strategy and the scan strategy. The specified variation of sensitivity with frequency results from a compromise among frequency coverage, survey duration, and sensitivity. It assumes that the angular rate at which the main beam of the antenna is swept across the celestial sphere is independent of the survey frequency. Because the beam area is inversely proportional to frequency squared, the duration of the survey is approximately proportional to the square of the highest frequency observed. If it were required that the sensitivity be independent of frequency, the scan rate would increase with frequency, and the duration of the survey would then be proportional to the cube of the highest frequency observed

A survey of the sky to a uniform limiting flux at any given frequency requires that the main beam of the antenna be swept across the celestial sphere at a rate that varies inversely as the square of the system temperature. The scan strategy is therefore designed to minimize the system temperature and its fluctuations, caused, for example, by changing sidelobe pickup and sky temperature variations. It must also utilize the antenna time efficiently, minimizing the time spent accelerating and decelerating and the time lost waiting for mechanical oscillations to damp out. Since SETI will not be the sole user of the antenna, it is necessary to subdivide the celestial sphere into elements which can be observed over the course of one to four hours and which are easily incorporated into a complete sky map with minimum overlap. Finally, the scan strategy must satisfy the requirements of the signal detector for signal confirmation and RFI rejection. In order to satisfy these conflicting requirements, we choose a reasonable survey time and design our strategy to achieve maximum sensitivity and uniformity. As shown below, our strategy requires that the scans be of moderate length and that successive scans be adjacent to one another.

Figure 1 is a schematic representation of one scan strategy which can satisfy these requirements using an alt-azimuth antenna. The pixels visible to the observatory are mapped by scanning the beam along lines of constant declination near transit. The maximum rate at which the antenna may be driven places an upper bound to the declination range for which this strategy may be employed and still yield a uniformly sensitive survey, since the required azimuth rate for this strategy varies inversely with the cosine of the declination. A different scan strategy must be employed at higher declinations. In general, a pixel will be mapped using a boustrophedonic scan pattern designed to optimize the system temperature by minimizing changes in elevation. A representative three-scan pattern is shown in the center of Fig. 1.

Although we desire to minimize the time lost reversing the direction of motion, care must be taken to avoid exciting the normal modes of oscillation of the mechanical system. Antenna dynamics and servo control time constants determine the duration of the turnaround period at the end of each scan. The scan length must not be so short that a large part of the time is wasted on the antenna turnaround.

## III. Signal Characteristics

If the number of independent samples included in the accumulation is large, the limiting sensitivity to a CW source achieved by accumulating over time $\tau$ as the antenna beam is swept through its position is:

$$\Phi(t,\tau) = \frac{4\alpha kT}{\pi\eta D^2}\sqrt{b/\tau}\;\frac{1}{\frac{1}{\tau}\int_{t}^{t+\tau} G(\psi)\,d\psi}\ \mathrm{W/m^2} \qquad (1)$$

where $\alpha$ is the signal to noise ratio (SNR) for detection, $T$ is the system temperature (K), $k$ is Boltzmann's constant (Watt-sec/K), $\eta$ is the aperture efficiency, $D$ is the diameter of the circular equivalent aperture (meters), and $b$ is the spectral resolution (Hz). The effective gain during the integration time is represented by the dimensionless function, $G(\psi)$, which is defined here to be unity when the source is on the beam axis. If the antenna beam tracks the source position rather than scanning through it, the integral becomes $\tau$ and the limiting sensitivity decreases as $1/\sqrt{\tau}$.

The time required to move the antenna beam through one half power beam width (HPBW) is approximately:

$$t_B = \frac{70c}{\nu D\omega} \qquad (2)$$

in seconds where $c$ is the speed of light (meter/sec), $\omega$ is rate in degrees/second at which the beam is swept across the sky (deg/sec), and $\nu$ is the frequency at which the survey is being carried out (Hz). The length of time that the source will be in the beam is approximately equal to $2t_B$, but the effective gain will vary greatly over that time interval.

Figure 2(a) shows the expected response within a frequency bin as the antenna beam is swept across the source position. For simplicity only a one dimensional slice of the circularly symmetric beam is shown. If the frequency response is measured as a source transits the beam, then the matched-filter detector would convolve the response with the beam shape shown. The ideal matched-filter would be many HPBWs long in order to use all the power from the source. It is desirable to find a practical filter length on the order of a HPBW. Figure 2(b) shows the SNR loss versus filter length in fractions of a HPBW. For lengths greater than 0.9 HPBW, the loss is less than 0.25 dB.

To keep the processing hardware cost-affordable, we accumulate spectra until there are only 3 to 5 spectra per HPBW. Figure 3(a) illustrates this coarser resolution and shows that the best SNR is realized when a source transits the center of the beam at the center of an accumulation interval. The worst case is when the maximum occurs at the transition between two accumulations. The uneven response due to this difference in source position is called scalloping. Figure 3(b) shows the SNR loss between the worst case and the best case for filter lengths of 1 HPBW and 0.6 HPBW. In both cases scalloping decreases as the number of accumulations increases.

## IV. The Signal Detection Strategy

The purpose of this section is to provide the background and theoretical basis for SETI sky survey signal detector performance evaluations. The problem is formulated as a classical binary decision problem of detecting a signal with random parameters in noise (Refs. 2, 3). Our treatment will rely, where applicable, on results to be found in the radar signal detection literature (Refs. 4, 5).

Figure 4 illustrates the basic front-end processing which is to be performed on the received signal. The ETI signal is assumed to be narrowband Continuous Wave (CW) of the form:

$$s(t) = A\cos(2\pi f_s t + \phi) \tag{3}$$

and the spectrum analyzer is assumed to have a resolution of 20 Hz. The detection system is designed to test for the two possibilities:

$$\begin{aligned} r(t) &= A\cos(2\pi f_s t + \phi), \quad \{H_1\} \\ r(t) &= n(t), \qquad\qquad\quad \{H_0\} \end{aligned} \tag{3a}$$

where $n(t)$ is a zero-mean Gaussian noise process whose variance, $\sigma_0^2$, is determined by the effective system temperature. Denoting by $x_j(f_\alpha)$ the $j$th sample of the $\alpha$th frequency bin, the accumulator output is given by:

$$\zeta_j(f_\alpha) = \sum_{n=0}^{N-1} |x_{Nj-n}(f_\alpha)|^2 \tag{4}$$

The probability density function (PDF) of the test statistic $\zeta$ under the null hypothesis $\{H_0\}$ is the gamma distribution with $2N$ degrees of freedom and $E\{\zeta\} = 2N$, $\sigma_\zeta^2 = 4N\sigma_0^2$. The PDF of $\zeta$ under the alternative hypothesis $\{H_1\}$ is the non-central chi-square distribution. The parameters of the PDF need to be explicitly related to the SETI observation parameters. In the receiver input with signal present, Eq. (3), if $A$ were constant, then the $\zeta_j$ would have the form:

$$q' = \sum_{i=1}^{N} (A + x_i')^2$$

where the $x_i'$ are identically distributed Gaussian random variables with zero mean and variance $\sigma_0^2$ (the system noise). However, under the conditions of the survey, the antenna scans at a relatively rapid rate and thus during the time required to accumulate $N$ samples ($T = N\tau$, where $\tau$ is the analyzer sample time), the received signal is modulated by the antenna beam pattern. We thus rewrite Eq. (3) as:

$$r(t) = A(t)\cos(2\pi f_s t + \phi) + n(t), \tag{5}$$

and note that the actual form of the $\zeta_i$ is now:

$$Q' = \sum_{i=1}^{N} (A_i + x_i')^2$$

Thus, from the results of Whalen (Ref. 2), the expression for $p_0(\cdot)$ is the chi-square distribution with $2N$ degrees of freedom:

$$p_0(\zeta) = \frac{1}{(\sigma_0^2)^N\, 2^N\, \Gamma(N)}\, \zeta^{N-1}\, e^{-\zeta/(2\sigma_0^2)} \tag{6}$$

and for $p_1(\cdot)$ is:

$$p_1(\zeta) = \frac{1}{2\sigma_0^2}\left(\frac{\zeta}{\lambda}\right)^{(N-1)/2} \exp\left[-(\zeta+\lambda)/2\sigma_0^2\right] I_{N-1}\left(\sqrt{\lambda\zeta}/\sigma_0^2\right) \tag{7}$$

with $2N$ degrees of freedom, where:

$$\lambda = 2\sum_{i=1}^{N} A_i^2$$

In Eq. (7), $I_N(\cdot)$ is the modified Bessel Function of the first kind and order $N$. These distributions are discussed in detail in Refs. 2 and 6.

We are now in a position to examine explicitly the effects of antenna scanning on $p_1(\cdot)$. The antenna scan rate is $\omega$ rad/sec, and the main lobe half-power beam width (HPBW) is $\Omega$ rad. The scan rate in HPBWs/sec is:

$$\nu \equiv \omega/\Omega \tag{8}$$

If $S_0$ represents the ETI signal flux at the surface of the earth in W/m$^2$, then

$$A(t) = \left(\frac{\pi D^2}{4}\,\epsilon S_0\right)^2 \exp\left(-\frac{1}{2}\left[\nu^2 (t-t_0)^2 + (\xi_2^0)^2/\Omega^2\right]\right) \tag{9}$$

where $D$ is the antenna diameter in meters, and $\epsilon$ is the antenna efficiency. A Gaussian main lobe shape has been assumed, and the coordinate system chosen, $(\xi_1, \xi_2)$, is centered on the moving bore-sight axis of the antenna, and $(\xi_1^0, \xi_2^0)$ denotes the actual source position. Thus, our expression for the $A_i$, which determines the non-central parameter, $\lambda$, is:

$$A_i^2 = \frac{\pi D^2}{4}\,\epsilon S_0 \times \frac{1}{\tau}\int_{t_i-\tau/2}^{t_i+\tau/2} \exp\left(-\left[\nu^2 (t-t_0)^2 + (\xi_2^0)^2/\Omega^2\right]\right) dt \tag{10}$$

This expression is rather cumbersome, so we make the simplifying assumption that $\tau \ll 1/\nu$, i.e., point-wise sampling, and rewrite Eq. (10) as:

$$A_i^2 = \frac{\pi D^2}{4}\,\epsilon S_0 \exp\left(-\left[\nu^2 (t-t_0)^2 + (\xi_2^0)^2/\Omega^2\right]\right) \tag{11}$$

Note that the $A_i$ have units of energy, so that the signal-to-noise ratio (SNR) for a single sample observation is:

$$SNR_i = \frac{A_i^2}{\sigma_0^2} \tag{12}$$

If we re-examine the expression for $\zeta_i$, Eq. (4), we see that the effect of antenna scanning is to produce weighted accumulation of individual samples, where the weight function, $w_i$, is just:

$$w_i = \exp\left\{-\left[\nu^2 (t_i - t_0) + (\xi_2^0)^2/\Omega^2\right]\right\} \tag{13}$$

From the above discussion, and our expression for $w_i$, it is apparent that for fixed $(\tau, \Omega, N)$ increasing the antenna scan rate above some value, $\omega_{max}$, reduces the accumulator performance to no better than single sample detection. In fact, an upper limit on scan rate may be set by choosing some minimum weight for the Nth sample as the antenna scans through a source. To illustrate the point, consider the case where the source position is $(\xi_1^0, \xi_2^0)$, $N$ is odd, and the center sample is taken with the source on beam-axis, i.e., $n = (N+1)/2$ at $\xi_1$. The weight function is rewritten with time in units of $n\tau$ as:

$$w_n = \exp\left[-\nu^2\tau^2 (n - (N+1)/2)^2\right], \qquad n = 1, 2, \cdots, N \tag{14}$$

Letting $\beta$ denote the minimum desired weight, from Eq. (14) we find

$$\omega_{max} = \frac{2\Omega}{\tau N}\left[\ln(1/\beta)\right]^{1/2} \tag{15}$$

or

$$\omega_{max} = \frac{0.6}{f_0 D\,\pi N}\left[\ln(1/\beta)\right]^{1/2} \tag{16}$$

where $f_0$ is the system operating frequency in GHz. Thus, for $D = 34$ meters, $f_0 = 1$ GHz, $\tau = 50$ ms, and $N = 8$, if we require $\beta = 0.5$, then $\omega_{max} = 10$ mrad/sec. On the other hand, at the upper end of the SETI survey frequency range, $f_0 = 10$ GHz, we have $\omega_{max} = 1.0$ mrad/sec which is significantly less than scan rate capabilities of the antenna system. Since $\tau$ is fixed and $\omega_{max}$ is only very weakly dependent on $\beta$, the dominating factor is our choice of $N$. For the time being we will assume that $\omega$ and $N$ may be suitably chosen so as to yield approximately uniform accumulator weighting; thus:

$$A^2 = \frac{\pi D^2}{4}\,\epsilon S_0 \tag{17}$$

and the non-central parameter appropriate for $p_1(\cdot)$, Eq. (7) is given by:

$$\lambda = 2NA^2 \tag{18}$$

We conclude our discussion of the statistics of $\zeta_i$ by casting the results obtained above in a form more amenable to computations described in Section IV. To accomplish this we introduce the "normalized" test statistics

$$q_0 = \sum_{i=1}^{N} \left( \frac{x_i'}{\sigma_0} \right)^2 \tag{19}$$

$$q_1 = \sum_{i=1}^{N} \left( \frac{A}{\sigma_0} + \frac{x_i'}{\sigma_0} \right)^2 \tag{20}$$

where the random variable $(x_i'/\sigma_0)$ is now zero-mean Gaussian with unit variance. The resulting PDFs under $H_0$ and $H_1$ are now given by (Ref. 2)

$$p_0(q) = \frac{1}{2^N \Gamma(N)} q^{N-1} \exp(-q/2) \tag{21}$$

with $2N$ degrees of freedom, $E\{q\} = 2N$, Var $\{q\} = 4N$; and

$$p_1(q) = \frac{1}{2} \left( \frac{q}{\lambda} \right)^{(N-1)/2} \exp[-(\lambda + q)/2] I_{N-1}(\sqrt{\lambda q}),$$

$$\lambda = \frac{2NA^2}{\sigma_0^2} \tag{22}$$

with $2N$ degrees of freedom, $E\{q\} = \lambda + 2N$, Var $\{q\} = 4(\lambda + N)$. Notice that, unlike the strictly Gaussian assumption sometimes used in detection problems, the presence of signal affects both the mean and variance of $p_1(\cdot)$.

For the purpose of performance prediction calculations we assume the ETI signal bandwidth to be much less than an analyzer bin-width, and that, if present, the signal is centered in a bin. These assumptions correspond roughly to Swirling's Case I model (Ref. 5). We will not discuss the effects of moving the signal within a bin in this article. We wish to examine the detection performance of several processing scenarios which cover a side range of cost and implementation complexity. The cases in this work are summarized in Fig. 5, and illustrated with data flow diagrams in Figs. 6-9.

## A. Case I

Referring to Fig. 6, we see that detection is carried out by applying a single threshold test to the individual $q_i(f_\alpha)$ This case corresponds most closely to the classical radar detection problem with noncoherent integration (Refs. 4, 5, 8). Since *a priori* probabilities cannot be realistically assigned for $H_0$ and $H_1$, we choose to use the Neyman-Pearson criterion for choosing our decision threshold. With the usual notation we define the probability of false alarm as:

$$P_{FA} = P(D_1 | H_0) = \int_{\gamma}^{\infty} p_0(q)\, dq \tag{23}$$

or

$$P_{FA} = 1 - F_0(\gamma; q) \tag{24}$$

where $F_0(\gamma; q)$ is the cumulative distribution function describing $H_0$, evaluated for $q = \gamma$; thus

$$F_0(\gamma; q) = \int_{\gamma}^{\infty} p_0(q)\, dq, \quad q \geq 0 \tag{25}$$

This later form is more useful for numerical computations (Refs. 4, 8, 9). Similarly the probability of detection is:

$$P_D = P(D_1 | H_1) = \int_{\gamma}^{\infty} p_1(q)\, dq \tag{26}$$

or, as above

$$P_D = 1 - F_1(\gamma; q) \tag{27}$$

Using the Neyman-Pearson criterion our threshold value, $\gamma$, is found from the required false alarm rate. Thus, we solve

$$\int_0^{\gamma} p_0(q)\, dq = 1 - \beta \tag{28}$$

where $\beta$ is the desired false alarm rate.

## B. Case II

Here we return to a discussion of the effects of antenna beam and shape and scan rate on our ability to detect an ETI source. A preliminary discussion of these effects for the case $N = 0$ (no accumulation) is described in Lockshin and Olsen (Ref. 10). The discussion leading up to Eq. (17) assumed that a scan strategy could be devised so that $N\tau \ll 1/\nu$. Thus, the

accumulator output gives us a sky sample every $N\tau$ seconds, or spatial sampling at "points" separated by $N\tau\omega$ radians. We will call this spacing the "intra-scan" separation.

$$\delta = N\tau\omega \text{ radians} \tag{29}$$

Intuitively it is clear that, given a finite $\Omega$, and assuming a uniform PDF for the spatial distribution of ETI sources, the probability of detection should be a monotonically decreasing function of $\delta$ using the test statistic $\zeta_i$ (or equivalently, $q_i$). Looked at from another viewpoint, for a given choice of $\delta$, the scanning operation cannot be accomplished at uniform sensitivity, an effect referred to as scalloping in Ref. 10. This means that for a source located between $\zeta_i$ and $\zeta_{i+1}$ the probability of detection will be less than if the source were at either $\zeta_i$ or $\zeta_{i+1}$.

In order to provide more uniform scan sensitivity, the accumulator output, after baseline correction, is passed through a convolutional filter as shown in Fig. 7. We thus have a new test statistic given by:

$$u_i = \sum_{m=0}^{M-1} a_m q_{i-m} \tag{30}$$

where the filter weights, $a_m$, are chosen to optimize $P_D$ over the sky area covered by the $M$ sample points. Due to the weighted sum in Eq. (30) the PDFs under $H_0$ and $H_1$ are no longer simply chi-square or non-central chi-square. Writing the test statistic as:

$$u = \sum_{i=1}^{M} a_i q_i \tag{31}$$

a single component, $u_j = a_j q_j$, has a PDF given by:

$$p(u_j) = \frac{1}{|a_j|}\, p(q_i/a_j)$$

Using the Fourier transform scaling property and the known characteristic functions for $p_0(q)$ and $p_1(q)$, the characteristic functions for $p_0(u)$ and $p_1(u)$ are found to be:

$$C_0(j\omega;u) = \prod_{i=1}^{M} \frac{1}{(1 - j\,2a_i\omega)^N} \tag{32}$$

and

$$C_1(j\omega;u) = \exp\left(-\frac{NMA^2}{2\sigma_0^2}\right) \times \exp\left(\sum_i^M \frac{NA^2\,\sigma_0^2/2}{[1 - j\,2a_i\,\sigma_0^2\,\omega]}\right) \times \prod_{i=1}^{M} \frac{1}{(1 - j\,2a_i\,\sigma_0^2\,\omega)^N} \tag{33}$$

As will be seen in Section IV it is not necessary to invert Eqs. (32) and (33) to obtain explicit expressions for $p_0(u)$ and $p_1(u)$. A discussion of weighted signal summation may be found in Di Franco and Rubin (Ref. 7). Since the test statistic $u$ is composed of $M$ samples covering a particular area of the sky, we actually need to compute:

$$p_1(u) = \iint_\Gamma p_1(u \mid \xi_1^0, \xi_2^0)\, p(\xi_1^0)\, p(\xi_2^0)\, d\,\xi_1^0\, d\,\xi_2^0 \tag{34}$$

where $(\xi_1^0, \xi_2^0)$ describes the source position. Here, $\{p(\xi_1^0)\, p(\xi_2^0)\}$ is the joint PDF describing the spatial distribution of sources, and is assumed to be uniform. The dependence of $p(u)$ on $(\xi_1^0, \xi_2^0)$ enters through the parameter $A$, which depends on intrascan separation, $\delta$, HPBW, and relative source position. The required detection probabilities can be computed without an explicit evaluation of Eq. (34).

### C. Case III

Further improvements in system performance can be obtained by combining observations from adjacent scan lines, i.e., "inter-scan line" signal combination. Case III represents an implementation of inter-scan line combination with a means for drastically reducing the amount of data storage required. Data decimation is achieved by "pre-thresholding" the convolutional filter output so as to allow only a certain percentage (on average) of the data to pass through for further processing. The pre-threshold level is set according to:

$$\int_{\gamma_p}^{\infty} p_0(u)\, du = \eta \tag{35}$$

where $\eta$ is the fraction of data allowed to pass threshold. By introducing inter-scan signal combination, we now have a test statistic which is bivariate, and in which each of the

marginal distributions is a thresholded version of $p_0(y)$, and $p_1(y)$. If we denote the test statistic after prethresholding by $u'$, then (Ref. 11),

$$p_i(u') = \begin{cases} p_i(u), & u > \gamma_p \\ p_i(\gamma_p)\,\delta(u-\gamma_p), & u = \gamma_p \\ 0, & u < \gamma_p \end{cases}, \quad i = 1, 2 \tag{36}$$

The behavior of this thresholding operation is illustrated in Fig. 10. As noted in Fig. 8, our test statistic, $u$, is a two-dimensional vector whose components are $\{u_k, u_{k+K}\}$. For notational convenience we will simply write $\vec{u} = (u'_1, u'_2)$ and remember that $u'_1$ and $u'_2$ refer to sample observations from adjacent scan lines. Now in order to determine the average system response to an ETI signal located somewhere in the area defined by the two vertically adjacent beam patterns, we assume a uniform spatial distribution of sources all of the same strength. Note that this result depends on vertical scan separation and beam profile, but not on scan rate.

If we denote by $\xi_1^0$ and $\xi_2^0$ the horizontal and vertical coordinates describing the location of an ETI source (see Fig. 11), then the joint PDF describing $\vec{u}$ is given by:

$$p_1(u'_1, u'_2) = \iint_\Gamma p_1(u_1|\xi_1, \xi_2)\, p_1(u_2|\xi_1, \xi_2) \times p(\xi_1)\, p(\xi_2)\, d\xi_1\, d\xi_2 \tag{37}$$

where the integration is carried out over the region $\Gamma$, as shown in Fig. 11. Since we are assuming uniform spatial distribution of source locations,

$$p(\xi_1)\, p(\xi_2) = 1/\Gamma$$

The explicit dependance of $p_1(u_i|\xi_1, \xi_2)$, $i = 1, 2$, on $(\xi_1, \xi_2)$ enters through the system response dependence on beam profile in a manner analogous to that shown by Eq. (7). Again assuming a Gaussian beam profile, the expression for $A(\xi_1, \xi_2)$ is given by:

$$A(\xi_1, \xi_2) = \frac{\pi D^2}{4}\, \epsilon S_0 \exp\left\{\frac{-2}{\Omega^2}\left[(\xi_1 - \xi_1^0)^2 (\xi_2 - \xi_2^0)^2\right]\right\} \tag{38}$$

The situation described above will be recognized as a problem in composite hypothesis testing for a bivariate random variable (Refs. 2, 12). Specifically, the null hypothesis is simple, while the alternative hypothesis is composite, being conditioned on the ETI source location parameters. Furthermore, since we are now dealing with a bivariate distribution, the decision regions, $R_0$ and $R_1$, are no longer divided by a single threshold value, but in fact by a family of such values which define a decision curve on the $(u'_1, u'_2)$-plane. The situation for a simple case is shown in Fig. 12, where the Neyman-Pearson curve is taken to be a quarter-circle; the region excluded by prethresholding is shaded.

### D. Case IV

For analysis purposes this case is identical to Case III except that we remove the prethresholding operation and allow the data to continue on to be combinatorially processed. A practical implementation of this case would of course require a very large amount of high-speed bulk storage and significantly increase processor speed requirements.

As can be seen from the above discussions, we have assumed a signal processing implementation which defers RFI and "natural source" identification operations to the very last processing step. This is not only useful for analysis purposes, but is in fact probably the only practical manner in which to implement a sky survey processing strategy. As a final note, we point out that all of our analyses assume that the "noise" is stationary, i.e., position independent. If this turns out to be a poor assumption, then the detection performance must be re-evaluated to incorporate adaptive threshold methods (Refs. 13, 18). The following section is devoted to describing in some detail the actual implementation of performance calculations carried out based on the problem formulation described in this section.

## V. Performance Analysis Calculations

In this section we wish to describe the methods used to carry out the required computations based on the discussion of Section III. The objective of these calculations is to produce a set of receiver operating characteristic (ROC) curves for each of the processing Cases (I-IV). These ROC curves will then be used to choose the signal processing strategy that yields the best performance/cost ratio. As has been pointed out in the literature (Refs. 8, 9, 14), numerical implementation of detection probability analyses encounters several practical difficulties. Some of these difficulties will be discussed before we proceed to describe the computational implementations actually used.

For our purposes, there are basically two computational issues to be addressed: (1) the use of Gaussian versus true PDFs; and (2) the choice of a numerical computation proce-

dure for the required probabilities. At first sight one might suspect, from the Central Limit Theorem, that Gaussian PDFs would provide an adequate approximation for our cases. However, we need to keep in mind that because of the small false alarm rate requirements ($<10^{-8}$), we are working very far out on the tails of distributions. Due to the relatively small number of samples involved ($<50$) one cannot expect the Gaussian to provide a very good approximation except near the "core" of the distribution. When using Gaussians to model the problem, we will use the means and variances computed from the actual non-central chi-square distributions as the Gaussian parameters. Regardless of the actual PDFs used, the choice of a numerical evaluation algorithm is critical in determining both solution accuracy, precision requirements, and computational time. Direct numerical integration of the PDFs invariably requires the use of extended computation precision and dynamic range and can result in excessively long CPU times (Refs. 8, 9) when one demands small false alarm rates.

We shall begin our discussion by setting out those elements of the computation that are common to all four cases. A general computation flow diagram is shown in Fig. 13. As pointed out in Section III, all variables are normalized by $\sigma_0^2$ so that the system noise PDF is zero-mean Gaussian with unit variance. The quantity $\sigma_0^2$ is determined solely by the effective system temperature and thus represents the noise energy at the receiver front-end. The SNRs used in computing the ROC curves are referred to the receiver front-end, and are defined as

$$S \equiv SNR = \frac{\pi D^2 \epsilon S_0}{4\sigma_0^2}, \qquad (39)$$

$$\sigma_0^2 = kT_s/\tau$$

where $k$ is Boltzmann's constant, and $T_s$ is the system temperature in Kelvin. In terms of the system parameters then:

$$S = \frac{\pi D^2 \epsilon \tau S_0}{4kT_s} \qquad (40)$$

In the numerical implementation of calculations described in this section all expressions for $P_{FA}$ and $P_D$ are parameterized in terms of $S$.

One of the more elegant and powerful methods for efficient numerical evaluation of detection probabilities has been described by Helstrom (Refs. 14, 15). Recalling the expressions for $P_{FA}$ and $P_D$ from Section III,

$$P_{FA} = 1 - F_0(\gamma; q) = 1 - \int_{-\infty}^{\gamma} p_0(q)\, dq \qquad (41)$$

$$P_D = 1 - F_1(\gamma; q) = 1 - \int_{-\infty}^{\gamma} P_1(q)\, dq \qquad (42)$$

and that the moment generating function (MGF) for $p(x)$ is defined by

$$\mu(\nu) = E\{e^{-\nu x}\} = \int_0^{\infty} p(x)\, e^{-\nu x}\, dx, \qquad x \geq 0 \qquad (43)$$

we may write a general expression for the required quantities using the inverse Laplace transform,

$$1 - F(\gamma; x) = L^{-1}\{\nu^{-1}[1 - \mu(\nu)]\} = \int_{c-i\infty}^{c+i\infty} \nu^{-1}[1 - \mu(\nu)]\, e^{\nu x} \frac{d\nu}{2\pi i} \qquad (44)$$

where the contour of integration is parallel to the imaginary axis and lies to the right of all poles in the integrand (Ref. 16). Helstrom's approach uses a saddlepoint integration (Ref. 17) technique to obtain an efficient approximation to the contour integral in Eq. (44). Taking the contour to the left of the origin, but still to the right of all singularities in the integrand, Eq. (44) may be expressed as

$$1 - F(\gamma; x) = \int_{c-i\infty}^{c+i\infty} -\nu^{-1}\, \mu(\nu)\, e^{\nu x}\, \frac{d\nu}{2\pi i}, \qquad c < 0 \qquad (45)$$

Using the fact that the integral in Eq. (45) is convex over $(-\infty < \nu < 0)$ the contour is placed so as to pass through $c = \nu_0$, i.e., $\nu = \nu_0 + iy$ $(-\infty < y < \infty)$, the point $\nu_0$ being the saddlepoint. Writing

$$\nu^{-1}\, \mu(\nu)\, e^{\nu x} = e^{\Phi(\nu)} \qquad (46)$$

and expanding $\Phi(\nu)$ as a Taylor series about $\nu_0$,

$$\Phi(\nu) = \Phi(\nu_0) + \frac{1}{2}\Phi''(\nu_0)(\nu - \nu_0)^2 + \cdots + \frac{1}{k!}\Phi^{(k)}(\nu - \nu_0)^k + \cdots \qquad (47)$$

the expression for $[1 - F(\gamma; x)]$ becomes

$$1 - F(\gamma; x) = -\nu_0^{-1} [2\pi\Phi''(\nu_0)]^{-1/2} \times \mu(\nu_0) e^{\nu_0\gamma} (1 + R), \qquad \nu_0 < 0 \quad (48)$$

where $R$ is the residual term given by Helstrom (Ref. 14). The saddlepoint is found simply by solving

$$\Phi'(\nu) = \frac{d}{d\nu} \ln [\mu(\nu)] + \gamma - \frac{1}{\nu} = 0 \quad (49)$$

numerically and noting that $\Phi(\nu)$ possesses only a single minimum ($\nu = \nu_0$) on the interval ($-\infty < \nu < 0$). As Helstrom points out, for $|E\{q\} - \gamma| \gg \sigma_q$, the residual term may be neglected and we shall use the zero-order approximation,

$$1 - F(\gamma; x) = -\nu_0^{-1} [2\pi\Phi''(\nu_0)]^{-1/2} \mu(\nu_0) e^{\nu_0\gamma}, \qquad \nu_0 < 0 \quad (50)$$

The threshold, $\gamma$, for a given choice of $P_{FA}$ is determined by an iterative solution of Eq. (50).

The treatment of Case II and Cases III and IV requires evaluation of conditional probabilities. As can be seen from Eqs. (21) and (36), direct evaluation of the integrals involved is quite tedius and such an approach would not allow us to take advantage of Helstrom's approximation technique. We therefore propose to treat these cases in the framework of a fluctuating target model (Ref. 5). The "fluctuation" is being induced by the antenna scan parameters and the assumption of a uniform spatial distribution for the probability of finding the source at a particular location within the area covered. Another view of Eqs. (31) and (37) is that the source position $(\xi_1^0, \xi_2^0)$ results in a conditioning of $p_1(\cdot)$ on $\lambda$, the non-central parameter.

Utilizing the above interpretation of the conditional probabilities encountered in Cases II-IV, we rewrite Eq. (43) as

$$\mu(\nu \mid \lambda) = \int_0^\infty p_1(q) e^{-\nu q} \, dq \quad (51)$$

where $p_1(q)$ is our non-central chi-square PDF with $N$ degrees of freedom and non-central parameter $\lambda$. Recall that $\lambda$ is in fact the total signal-to-noise ratio at the output of the convolutional filter. For the given PDF, Eq. (51) yields (Ref. 14)

$$\mu(\nu \mid \lambda) = (1 + \nu)^{-N} \exp [-\lambda\nu/(1 + \nu)] \quad (52)$$

Denoting by $p_\lambda(\lambda \mid \bar{\lambda})$ the PDF of $\lambda$ which describes the fluctuation model, the unconditional MGF is obtained from

$$\mu(\nu) = \int_0^\infty \mu(\nu \mid \lambda) p_\lambda(\lambda \mid \bar{\lambda}) \, d\lambda \quad (53)$$

With suitable change of variable, Eq. (53) is seen to be the Laplace transform of $p_\lambda(\cdot)$ and thus the unconditional MGF is

$$\mu(\nu) = (1 + \nu)^{-\nu} \mu_\lambda [\nu/(1 + \nu)] \quad (54)$$

where $\mu_\lambda[\cdot]$ is the MGF of the distribution describing our fluctuation model. Therefore, given a suitable fluctuation model which yields $\mu_\lambda[\cdot]$ in analytic form, we may utilize the saddlepoint method to compute approximate detection probabilities for Cases II-IV.

Recalling the discussion and assumptions leading up to Eq. (17) in Section III, our Case II appears to formally correspond to the Swerling model I. In practice the situation actually lies somewhere between Swerling I and II. For simplicity we take our fluctuation model PDF to be (Ref. 5)

$$p_\lambda(\lambda \mid \bar{\lambda}) = \frac{1}{\bar{\lambda}} \exp(-\lambda/\bar{\lambda}) \quad (55)$$

where $\bar{\lambda}$ is computed by averaging the antenna response over the area covered by our $M$-point convolution of Eq. (28). Note that this averaging process includes the convolutional weights for each of the $M$ samples. Cases III and IV are treated in the same way, the obvious extension to bivariate distributions.

Finally we note that the MGF describing the test statistics used in Cases II-IV, can be derived in a manner similar to that used in finding the characteristic functions, Eqs. (32) and (33). Thus, for Case II the MGF's under $\{H_0\}$ and $\{H_1\}$ are given by

$$\mu_0(\nu) = \prod_{i=1}^{M} (1 + a_i \nu)^{-N} \quad (56)$$

and

$$\mu_1(\nu) = \exp \left[ -\sum_{i=1}^{M} \frac{a_i \lambda \nu}{(1 + a_i \nu)} \right] \prod_{i=1}^{M} (1 + a_i \nu)^{-N} \quad (57)$$

where, as before, the $a_i$ denote the convolutional filter weights. Here it is most convenient to use the cumulant generating function, $h(\nu) = \ln \mu(\nu)$ and we then have

$$h_0(\nu) = -N \sum_{i=1}^{M} \ln (1 + a_i \nu) \quad (58)$$

and

$$h_1(\nu) = -\sum_{i=1}^{M} \frac{a_i \lambda \nu}{(1 + a_i \nu)} - N \sum_{i=1}^{M} \ln (1 + a_i \nu) \quad (59)$$

Results of our performance calculations for the Gaussian model are shown in Fig. 14 and 15, for $P_{FA}$ of $10^{-12}$ and $10^{-8}$ respectively. For an assumed antenna temperature of 25 K, an SNR ratio of 1 is equivalent to a received flux of approximately $2 \times 10^{-23}$ W/m$^2$ at the antenna. The relative performance of the four cases studied is easily seen from these Receiver Operating Characteristic (ROC) curves. The largest increase in performance comes in going from Case I to Case II, where we add intra-scan combination processing. As is to be expected, there is little difference in performance between Cases III and IV; both cases yielded a performance increase of about a factor of two over that for Case II. A similar set of ROC calculations is currently being carried out using the actual chi-square distributions which describe the problem and will be reported in a later paper.

## References


1. Wilck, H. C., Quirk, M. P., Grimm, M. J., "A Wide-Band, High-Resolution Spectrum Analyzer," *The Telecommunications and Data Acquisition Progress Report 42-83*, The Jet Propulsion Laboratory, Pasadena, CA, 1985.
2. Whalen, A. D., *Detection of Signals in Noise*, Academic Press, New York, 1971.
3. Helstrom, C. W., *Statistical Theory of Signal Detection*, Pergamon Press, New York, 1968.
4. Marcum, J. I., and Swerling, P. A., "A Statistical Theory of Target Detection by Pulsed Radar," *IRE Trans. Inform. Theory*, IT-6, 59-267 (April 1960).
5. Swerling, P. A., "Probability of Detection for Fluctuating Targets," *IRE Trans. Inform. Theory*, IT-6, 269-308 (April, 1960).
6. Patnaik, P. B., "The Non-Central Chi-Square and F-distributions and their Applications," *Biometrika*, 36, 202 (1949).
7. DiFranco, J. V., and Rubin, W. L., *Radar Detection*, ARTECH House, Inc., Dedham, MA, 1980.
8. Bird, J. S., "Calculating Detection Probabilities for Systems Employing Noncoherent Integration," *IEEE Trans. on Aerospace and Electronic System*, AES-18, 401-409 (July, 1982).
9. Helstrom, C. W., and Ritcey, J. A., "Evaluating Radar Detection Probabilities by Steepest Descent Integration," *IEEE Trans. Aerospace and Electronic Systems*, AES-20, 624-633 (September, 1984).
10. Loksin, A. and Olsen, E. T., "An Investigation of the Effects of Scan Separation on the Sensitivity of the SETI All Sky Survey for the Case of Gaussian Noise," *TDA Progress Report* 42-77, pp. 151-158, Jet Propulsion Laboratory, Pasadena, CA, Mar. 1984.
11. Papoulis, A., *Probability, Random Variables, and Stochastic Processes*, Chap. 5, McGraw-Hill, New York, 1965.

12. Lehman, E. L., *Testing Statistical Hypotheses*, Wiley, New York, 1959.

13. Bird, J. S., "Calculating Detection Probabilities for Adaptive Thresholds," *IEEE Trans. Aerospace and Electronic Systems*, AES-19, 506-512 (July 1983).

14. Helstrom, C. W., "Approximate Evaluation of Detection Probabilities in Radar and Optical Communications," *IEEE Trans. Aerospace and Electronic Systems*, AES-14, 630-640 (July 1978).

15. Helstrom, C. W., "Evaluating the Detectability of Gaussian Stochastic Signals by Steepest Descent Integration," *IEEE Trans. Aerospace and Electronic Systems*, AES-19, 428-437, (May 1983).

16. Feller, W., *An Introduction to Probability Theory and its Applications*, Vol. II, Chap. XIII, (John Wiley, New York, 1971).

17. Jeffreys, H., *Asymptotic Approximations*, Oxford Univ. Press., London, 1962.

18. Nitzberg, R., "Constant-False-Alarm-Rate Signal Processors for Several Types of Interference," *IEEE Trans. Aerospace and Electronic Systems*, AES-8, 27-34, (Jan. 1972).

**Table 1. Characteristics of the All Sky Survey (for a 34-m parabolic antenna)**

| | |
|---|---|
| Spatial Coverage | $4\pi$ steradians |
| Frequency Coverage | 1–10 GHz and higher spot bands |
| Duration of Survey | 5–10 years |
| Dwell Time on Source | 0.5–10 seconds |
| Frequency Resolution | 10–30 Hz |
| Sensitivity | $\approx 10^{-23}$ Watts/meter$^2$ |
| Spatial Uniformity | 12% peak-to-peak |
| Variation with Frequency | $\approx \nu^{1/2}$ |
| Polarization | Simultaneous Dual Circular |
| Signal Type | Continuous Wave (CW) |

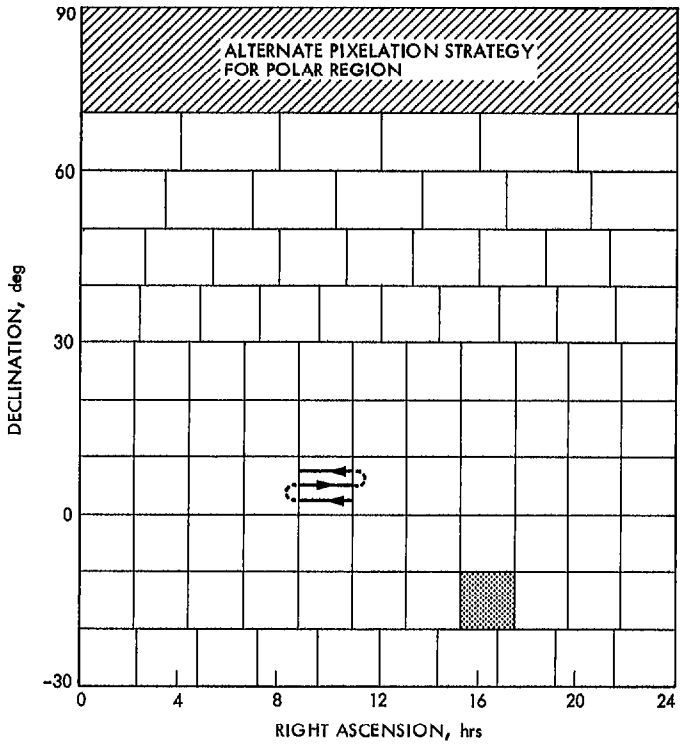


**Fig. 1. Schematic representation of sky pixelation and scan strategy**

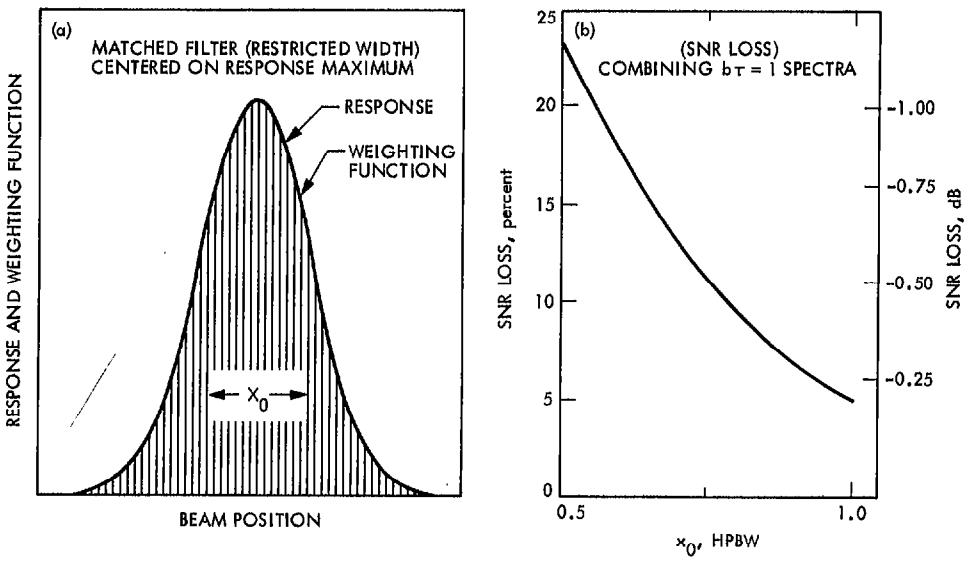


**Fig. 2. Antenna scan effects: (a) the expected response within a frequency bin as the antenna beam is swept across a source; (b) the SNR loss as a function of filter length, $X_0$, in HPBWs**

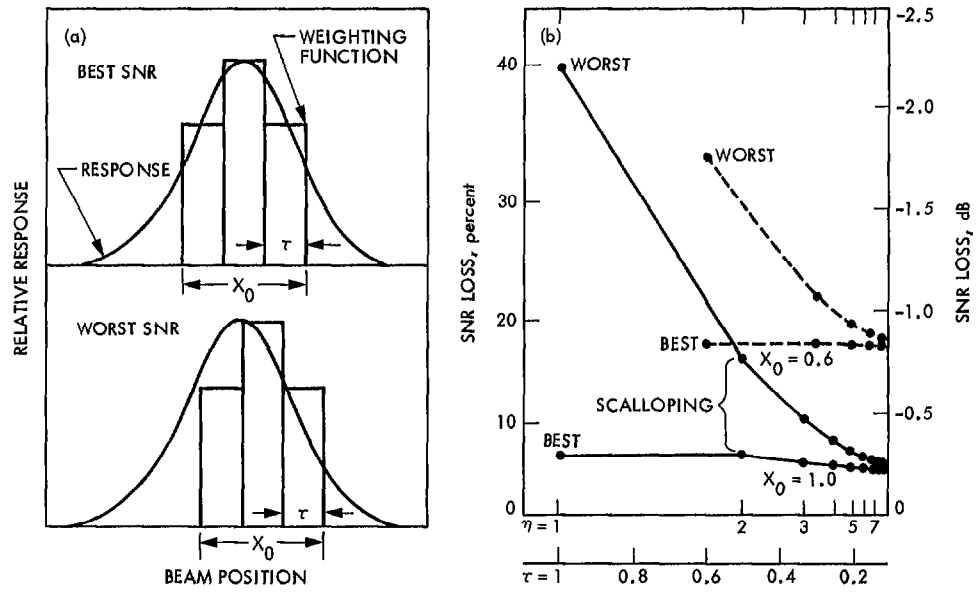


**Fig. 3. Scalloping effects: (a) Schematic representation of the source of scalloping; (b) variation of SNR loss**

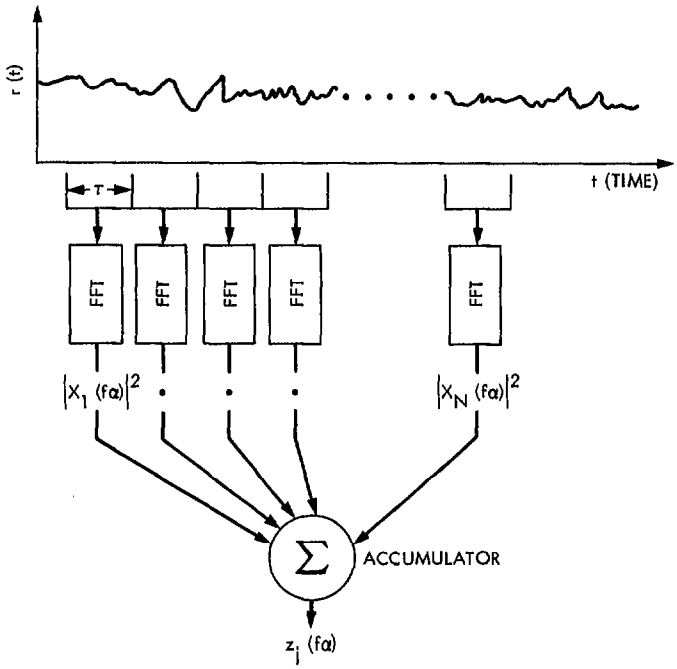


**Fig. 4. Front-end signal processing**

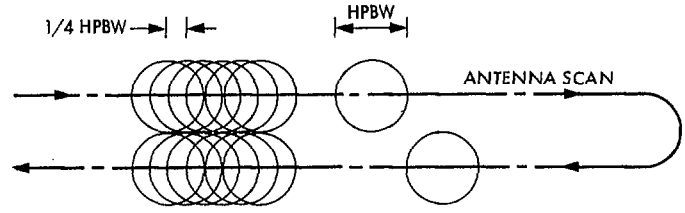


CASE I: APPLY THRESHOLD DETECTION (NEYMAN-PEARSON) DIRECTLY TO BASELINE CORRECTED DATA; DO NOT USE INTRA- OR INTER-SCAN LINE COMBINATIONS

CASE II: APPLY FOUR-POINT CONVOLUTIONAL FILTER TO SUCCESSIVE SAMPLES OF BASELINE CORRECTED DATA PRIOR TO APPLYING THRESHOLD DETECTION; ACHIEVES INTRA-SCAN LINE COMBINATION TO REDUCE SCALLOPING

CASE III: EXTENDS CASE II TO ACHIEVE INTER-SCAN LINE COMBINATION, BUT APPLIES "PRE-THRESHOLDING" TO REDUCE DATA RATES

CASE IV: RETAINS ALL ACQUIRED DATA NECESSARY TO ACHIEVE INTER-SCAN LINE COMBINATION PROCESSING

**Fig. 5. Signal processing scenarios**

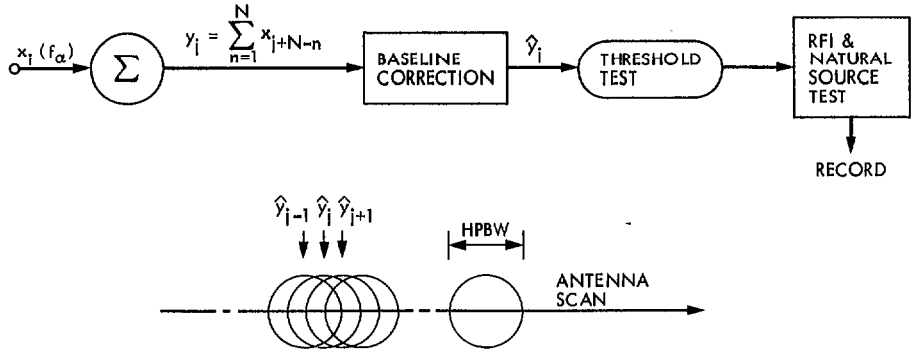


**Fig. 6. Signal processing, Case I**

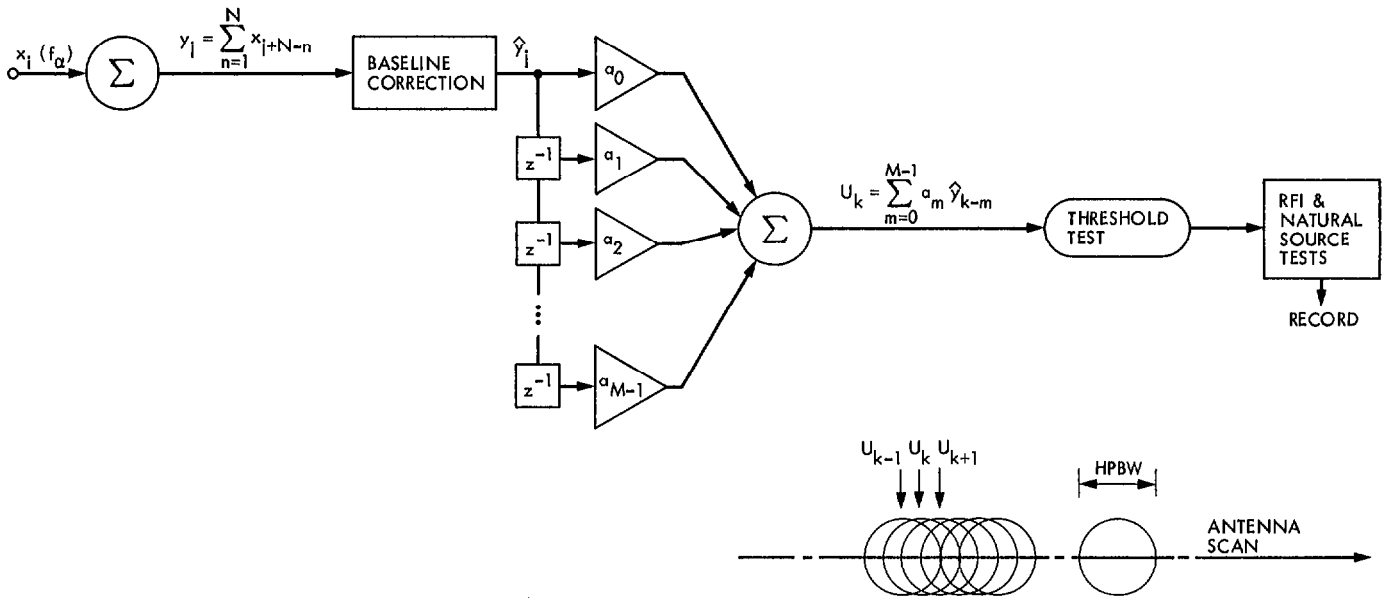


**Fig. 7. Signal processing, Case II**

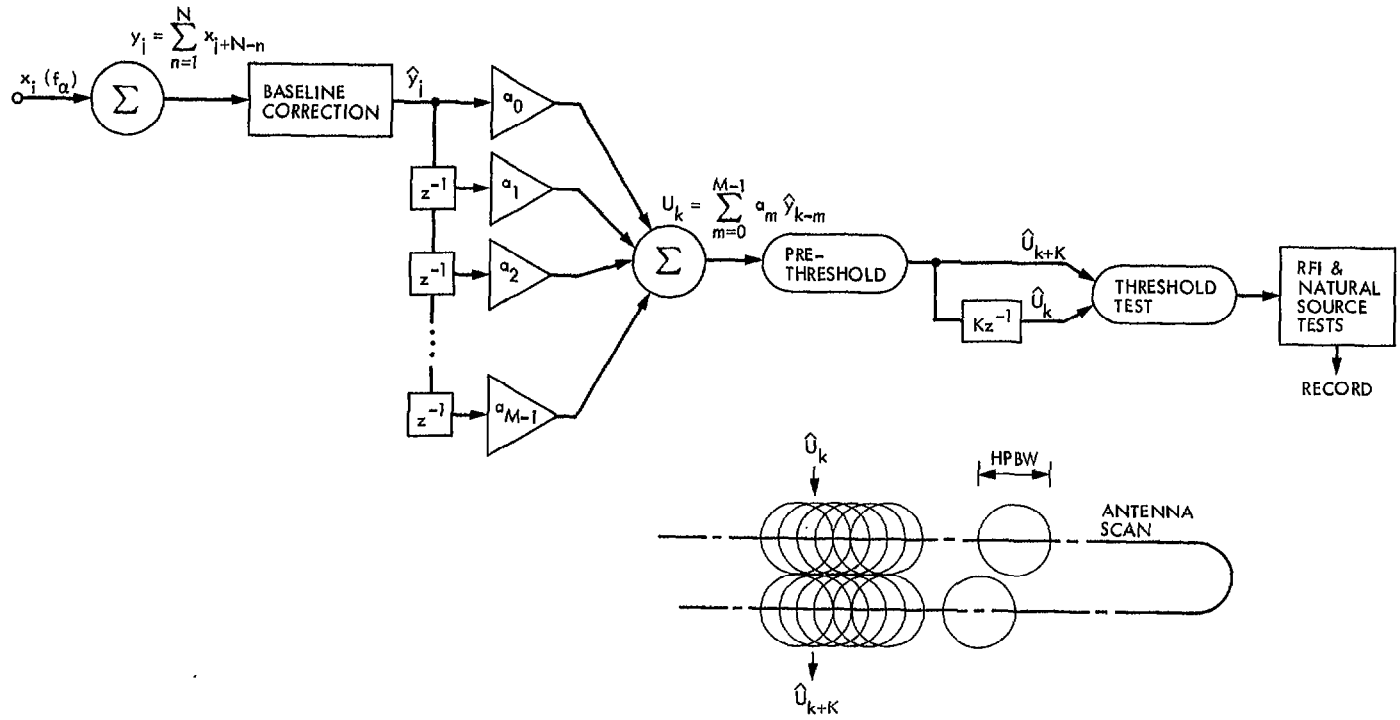


**Fig. 8. Signal processing, Case III**

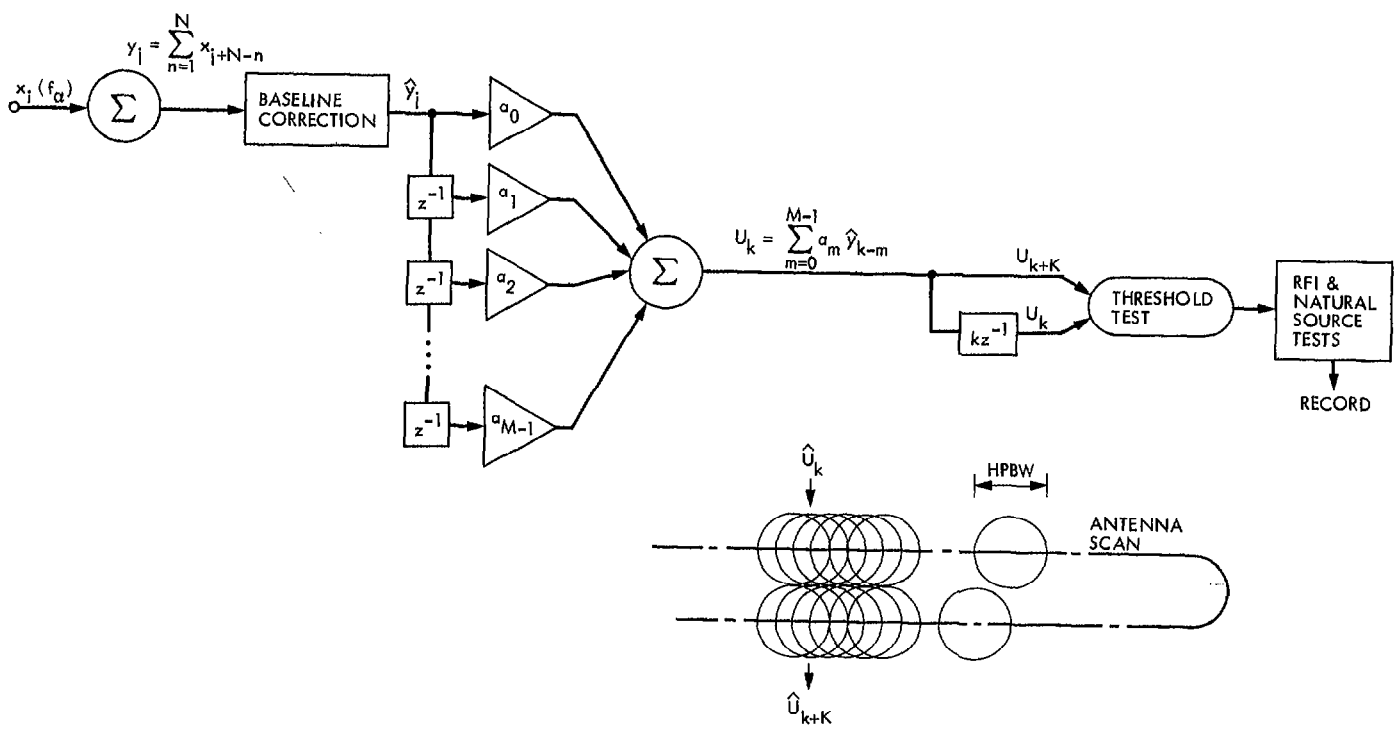


**Fig. 9. Signal processing, Case IV**

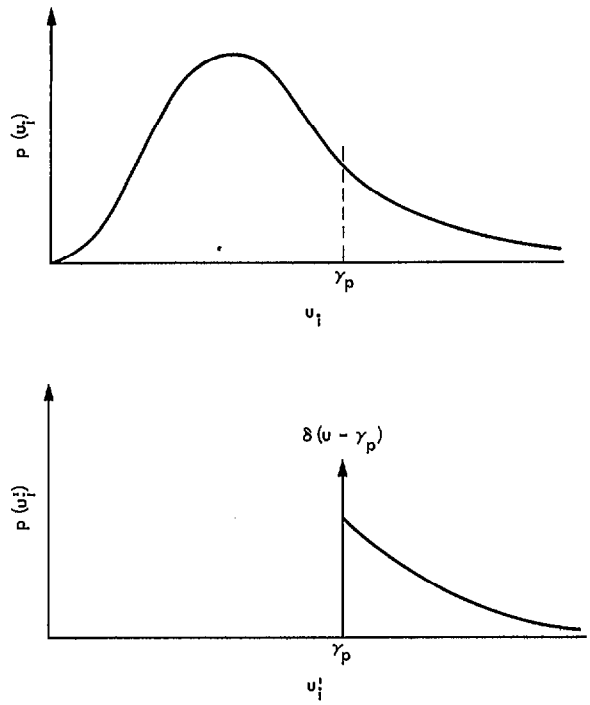


Fig. 10. Effects of the thresholding operation

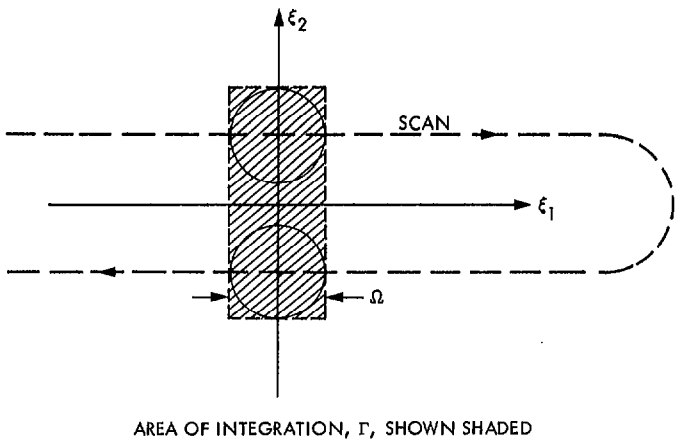


AREA OF INTEGRATION, Γ, SHOWN SHADED

Fig. 11. Inter-scan combination geometry

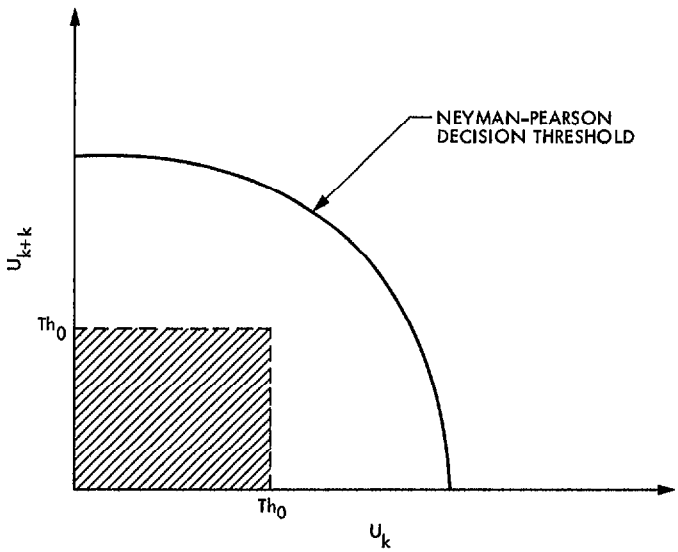


Fig. 12. Inter-scan combination case

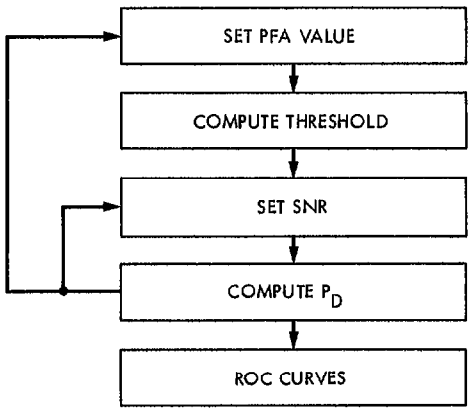


Fig. 13. Computational flow

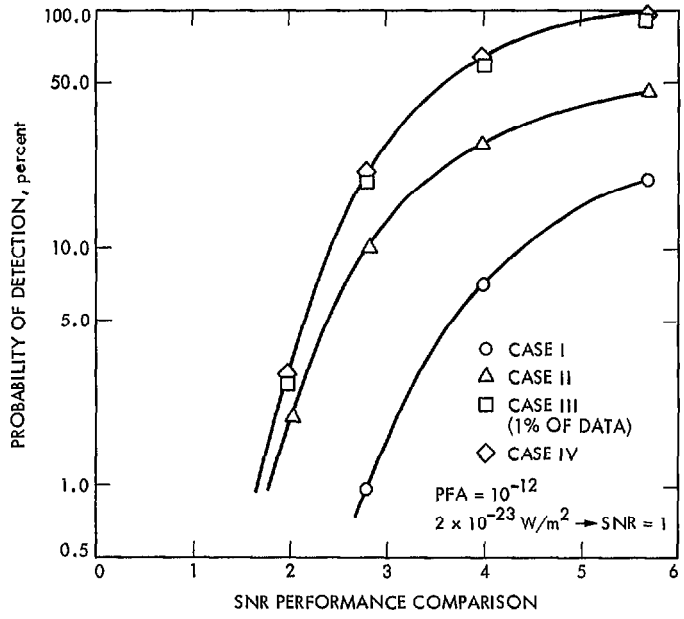


**Fig. 14. Receiver operating characteristic curves for PFA = $10^{-12}$**

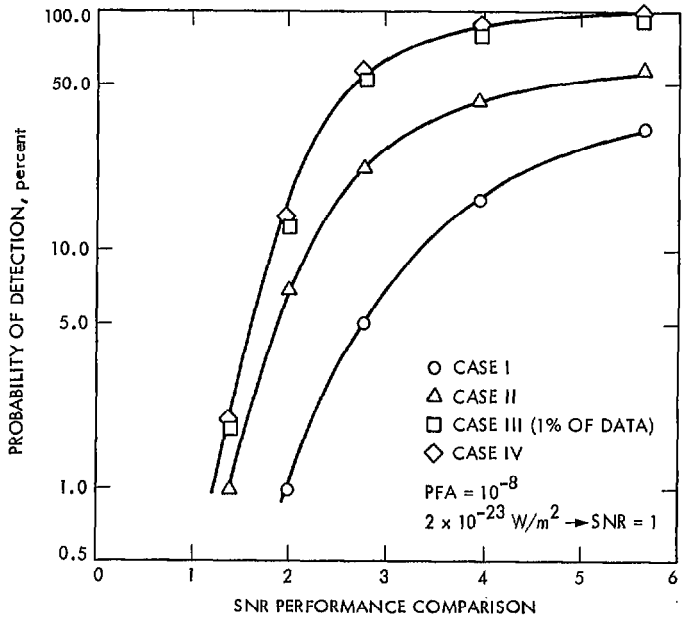


**Fig. 15. Receiver operating characteristic curves for PFA = $10^{-8}$**